Stretching and Buckling of Small Elastic Fibers in Turbulence

Sofía Allende, Christophe Henry, and Jérémie Bec
Université Côte d'Azur, CNRS, OCA, Laboratoire J.-L. Lagrange, 06300 Nice, France

Small flexible fibers in a turbulent flow are found to be as straight as stiff rods most of the time. This is due to the cooperative action of flexural rigidity and fluid stretching. However, fibers might bend and buckle when they tumble and experience a strong enough local compression. Such events are similar to an activation process, where the role of temperature is played by the inverse of Young's modulus. Numerical simulations show that buckling occurs very intermittently in time. This results from unexpected long-range Lagrangian correlations of the turbulent shear.

Elongated colloidal particles are essentially subject to three forces: bending elasticity, thermal fluctuations, and viscous drag with the suspending flow. An important and well-studied case is that of infinitely flexible polymers for which only two effects compete: coiling promoted by thermal noise and stretching induced by fluid shear. Relaxation to equilibrium is then fast enough to give grounds for adiabatic macroscopic models, such as elastic dumbbells [1,2], often used to investigate the rheology of polymer suspensions [3]. Much less is known about when the thermal fluctuations are negligible but bending elasticity becomes important. This asymptotics is relevant to describe macroscopic particles, such as cellulose fibers in the paper making industry [4], or diatom phytoplankton colonies [5] that significantly participate in the CO_2 oceanic pump [6]. In principle, without molecular diffusion there is no coiling. Furthermore, bending elasticity and flow stretching act concomitantly to straighten the fiber, suggesting an unsophisticated stiff rod dynamics. However, most natural or industrial flows are turbulent. They display violent and intermittent fluctuations of velocity gradients, susceptible of destabilizing a straight configuration by buckling the fiber [7].

We are interested in elongated, deformable, nondiffusive particles passively transported by a turbulent flow. We aim at quantifying two aspects: first, the extent to which their dynamics can be approximated as that of rigid rods and, second, the statistics of buckling. For that purpose, we focus here on the simplest model, the *local* slender-body theory, which describes the motion of an inextensible Euler-Bernoulli beam immersed in a viscous fluid. In the limit of zero inertia, the fiber velocity is obtained by equating the drag, the tension, and the bending elasticity (see, e.g., Ref. [8]). The dynamics of a fiber with cross section a and length ℓ is then

$$\partial_t X = u(X, t) + \frac{c}{8\pi\rho_f\nu}\mathbb{D}[\partial_s(T\partial_s X) - E\partial_s^4 X],$$

$$|\partial_s X|^2 = 1, \quad \text{with} \quad \mathbb{D} = \mathbb{I} + \partial_s X \partial_s X^\mathsf{T}, \tag{1}$$

in the asymptotics $c = -[1 + 2\log(a/\ell)] \gg 1$. Here, $X(s, t)$ is the spatial position of the point indexed by the arc length coordinate $s \in [-\ell/2, \ell/2]$, u is the velocity field of the fluid, ν its kinematic viscosity, ρ_f its mass density, and E denotes the fiber's Young modulus. The tension $T(s, t)$, which satisfies $T|_{\pm\ell/2} = 0$, is the Lagrange multiplier associated to the fiber's inextensibility constraint. Equation (1) is supplemented by the free-end boundary conditions $\partial_s^2 X|_{\pm\ell/2} = 0$ and $\partial_s^3 X|_{\pm\ell/2} = 0$.

The considered fibers are much smaller than the smallest active scale of the fluid velocity u. In turbulence, this means $\ell \ll \eta$, where $\eta = \nu^{3/4}/\varepsilon^{1/4}$ is the Kolmogorov dissipative scale, $\varepsilon = \nu\langle\|\nabla u\|^2\rangle$ being the turbulent rate of kinetic energy dissipation. In this limit, the particle motion is to leading order that of a tracer and $d\bar{X}/dt = u(\bar{X}, t)$, where $\bar{X}(t)$ denotes its center of gravity. The deformation of the fiber solely depends on the local velocity gradient, so that $u(X, t) \approx u(\bar{X}, t) + \mathbb{A}(t)(X - \bar{X})$, where $\mathbb{A}_{ij}(t) = \partial_j u_i(\bar{X}, t)$. The dynamics is then fully described by two parameters: the fluid flow Reynolds number Re, prescribed very large, and the nondimensional fiber flexibility, defined as

$$\mathcal{F} = \frac{8\pi\rho_f\nu\ell^4}{cE\tau_\eta}, \tag{2}$$

where $\tau_\eta = \sqrt{\nu/\varepsilon}$ is the Kolmogorov dissipative time and quantifies typical values of the turbulent strain rate. The parameter $\mathcal{F}$ can be understood as the ratio between the timescale of the fiber's elastic stiffness to that of the turbulent velocity gradients. At small $\mathcal{F}$, the fiber is very rigid and always straight. On the contrary, for large $\mathcal{F}$ it is very flexible and might bend. Clearly, if the fiber had inertia, the dynamics would involve its material density and depend on an extra parameter (e.g., the Stokes number). This would probably affect bending properties.

In the straight configuration, the tangent vector is constant along the fiber, i.e., $\partial_s X = \mathbf{p}(t)$, and follows Jeffery's equation for straight ellipsoidal rods [9]:

$$\frac{d\mathbf{p}}{dt} = \mathbb{A}\mathbf{p} - (\mathbf{p}^{\mathsf{T}}\mathbb{A}\mathbf{p})\mathbf{p}. \tag{3}$$

This specific solution to Eq. (1), which is independent of s, is stable when the fiber is sufficiently rigid. However, it becomes unstable when increasing flexibility, or equivalently for larger fluid strain rates. As shown and observed experimentally in two-dimensional velocity fields, such as linear shear [7,10,11] or extensional flows [12–14], this instability is responsible for a buckling of the fiber. This occurs when the elongated fiber tumbles [15,16] and experiences a strong enough compression along its direction. This compression is measured by projecting the velocity gradient along the rod directions, i.e., by the stretching rate $\dot{\gamma} = \mathbf{p}^{\mathsf{T}}\mathbb{A}\mathbf{p}$. In turbulence, buckling thus occurs when the instantaneous value of $\dot{\gamma}$ becomes large with a negative value (compression).

To substantiate this picture, we have performed direct numerical simulations of three-dimensional homogeneous isotropic turbulence. The flow is obtained by integrating the incompressible Navier-Stokes equations using the LATU spectral solver with 4096^3 collocation points and a force that keeps kinetic energy constant in the two first Fourier shells [17]. Once a statistically steady state is reached with a Taylor microscale Reynolds number, $\mathrm{Re}_\lambda \approx 730$, the flow is seeded with several millions of tracers, along which the full velocity gradient is stored with a period $\approx \tau_\eta/4$ during four large-eddy turnover times (up to $t \simeq 734\tau_\eta$). The local slender-body equation for fibers, Eq. (1), is then integrated *a posteriori* along a subset of 4000 tracer trajectories uniformly distributed in the domain, and eight different values of the flexibility. We use the semi-implicit, finite-difference scheme of Ref. [9], with the inextensibility constraint enforced by penalization. $N = 201$ grid points are used along the fiber arc length, with a time step $5 \times 10^{-4}\tau_\eta$. We use linear interpolation in time to access the velocity gradient at a higher frequency than the output from the fluid simulation.

Numerics confirm that fibers much smaller than the Kolmogorov scale are almost always straight. This can be measured from the end-to-end length $R(t) = |\mathbf{X}(\ell/2, t) - \mathbf{X}(-\ell/2, t)|$. When $R = \ell$, the fiber has a rod shape. Buckling occurs when $R < \ell$. The upper panel of Fig. 1 shows the time evolution of the end-to-end length along a single trajectory for various nondimensional flexibilities $\mathcal{F}$. Clearly, bending is sparse and intermittent. Buckling events are separated by long periods during which $R \equiv \ell$, up to numerical precision. For instance, one observes $|1 - R(t)/\ell| < 10^{-13}$ in the time interval $100 < t/\tau_\eta < 180$. In the lower panel of Fig. 1, we have shown the time evolution of the stretching rate $\dot{\gamma}$ along the same Lagrangian trajectory. As expected, buckling events are associated with strong negative fluctuations of $\dot{\gamma}$. Note that, because $\mathbf{p}$ is preferentially aligned with the fluid stretching [18], the rate $\dot{\gamma}$ has a positive mean $\langle\dot{\gamma}\rangle \approx 0.11/\tau_\eta$. Its standard deviation is $\approx 0.2/\tau_\eta$.
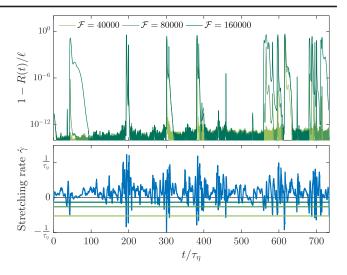

FIG. 1. Top: Time evolution of the end-to-end length $R(t)$ for a specific turbulent tracer trajectory and three different values of the nondimensional flexibility $\mathcal{F}$, as labeled. Bottom: Evolution of the instantaneous stretching rate $\dot{\gamma}$ along the same trajectory. The solid lines correspond to $\tau_\eta\dot{\gamma} = 0, -0.13, -0.26$, and -0.52. Note that time is rescaled by the Kolmogorov timescale τ_η. In these units, the large-eddy turnover time is $\tau_L \approx 190\tau_\eta$.

To get more quantitative insight, we define buckling events as times when $R(t)/\ell$ is below a prescribed threshold (we have used 0.999). Figure 2 shows the probability of buckling as a function of the flexibility $\mathcal{F}$. This quantity, denoted Φ, is defined as the fraction of time spent by the end-to-end length below this threshold. Conversely to
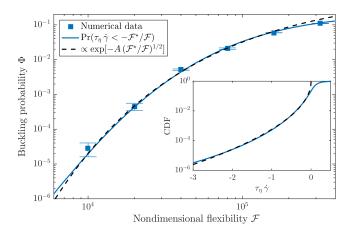

FIG. 2. Probability of buckling Φ as a function of $\mathcal{F}$. The squares come from numerical simulations and were calculated as the fraction of time during which $R(t)/\ell < 0.999$. Error bars show the standard deviation of these estimates, obtained when assuming that buckling events are uncorrelated. The bold line is the probability that the stretching rate $\dot{\gamma}$ is less than $-\mathcal{F}^\star/(\tau_\eta\mathcal{F})$ with $\mathcal{F}^\star = 2.1 \times 10^4$. The corresponding cumulative distribution function (CDF) is shown in the inset, together with a fit (dashed line) of the form $\propto \exp[-A(\tau_\eta|\dot{\gamma}|)^{1/2}]$, where $A = 1.69$. The same approximation is used in the main panel to fit Φ (dashed line).

simple steady shear flows (see, e.g., Ref. [8]), and differently from what is observed for long fibers in turbulence [19,20], here we find that there is no critical value of the flexibility above which buckling occurs. Fibers bending is similar to an activated process with $\Phi \propto \exp(-C/\mathcal{F}^\alpha)$ and where the flexibility $\mathcal{F}$ plays a role resembling that of temperature in chemical reactions. Indeed, the fiber is found to buckle when its instantaneous flexibility $\mathcal{F}_{\mathrm{loc}}(t) = \tau_\eta |\dot{\gamma}(t)| \mathcal{F}$ is larger than a critical value $\mathcal{F}^\star$, with $\dot{\gamma}(t) < 0$. This leads to

$$\Phi = \Pr\left(\tau_\eta \dot{\gamma} < -\mathcal{F}^\star/\mathcal{F}\right). \qquad (4)$$

As can be seen in Fig. 2, the cumulative probability of the stretching rate can indeed be used to reproduce the numerical measurements of Φ by choosing $\mathcal{F}^\star = 2.1 \times 10^4$. This value, which just corresponds to a fit, is much larger than those observed in time-independent shear flows [11] where buckling occurs for $\mathcal{F} \gtrsim 300$. A first reason comes from using the Kolmogorov dissipative timescale when defining $\mathcal{F}$. This is a natural but arbitrary choice in turbulence. However, τ_η is significantly smaller than typical values of $\dot{\gamma}^{-1}$, so that effective flexibilities could be smaller than $\mathcal{F}$. This is similar to choosing τ_η rather than the Lyapunov exponent to define the Weissenberg number for the coil-stretch transition of dumbbells in turbulent flow [21]. Another explanation for a large $\mathcal{F}^\star$ could be the intricate relation in turbulence between the amplitude of velocity gradients and their dynamical timescales, which implies in principle that the stronger $\dot{\gamma}$ is, the shorter the lifetime of the associated velocity gradient.

Fibers with a small flexibility buckle only when the instantaneous stretching rate is sufficiently violent. Moreover, it is known that at large Reynolds numbers [22], the probability distribution of velocity gradients has stretched-exponential tails with exponent $\approx 1/2$. This behavior is also present in the cumulative probability of $\dot{\gamma}$, as seen in the inset of Fig. 2. This leads to the prediction that

$$\Phi \propto e^{-A(\mathcal{F}^\star/\mathcal{F})^{1/2}} \quad \text{for } \mathcal{F} \ll \mathcal{F}^\star. \qquad (5)$$

This asymptotic behavior is shown as a dashed line in the main panel of Fig. 2. It gives a rather good fit of the data, up to $\mathcal{F} \approx 1.6 \times 10^5$. At larger values, this activationlike asymptotics and relation to the tail of the distribution is no longer valid. At very small values (or equivalently large negative $\dot{\gamma}$'s), one observes tiny deviations from the stretched exponential, certainly resulting from numerical errors overpredicting extreme gradients [23].

The relevance to buckling of an instantaneous flexibility larger than $\mathcal{F}^\star$ can be seen in Fig. 1. The dashed lines in the bottom panel are the critical values $\tau_\eta \dot{\gamma} = -\mathcal{F}^\star/\mathcal{F}$ associated to the three flexibilities of the top panel. We indeed observe that buckling occurs when the instantaneous stretching rate underpasses these values. In some cases

(e.g., for times between 400 and $500\tau_\eta$), it seems that the fiber is straight, even if $\dot{\gamma}$ is below the threshold. Still, buckling occurs but with an amplitude so small that it cannot be detected from the top panel. This threshold therefore provides information on the occurrence of buckling, but not on the strength of the associated bending.

Another qualitative assessment that can be drawn from Fig. 1 is that large excursions of $\dot{\gamma}$ are not isolated events but form clumps. This is a manifestation of the Lagrangian intermittency of velocity gradients. Tracers might indeed be trapped for long times in excited regions of the flow, leading to fluctuations correlated over much longer times than τ_η. This can be quantified from the autocorrelation $\rho(t)$ of the negative part $\dot{\gamma}^- = \max(-\dot{\gamma}, 0)$ of the stretching rate, which is represented in the inset of Fig. 3. The corresponding integral correlation time is $\int \rho(t)dt \approx 2.8\tau_\eta$. This can be explained by the abrupt decrease of the autocorrelation at times of the order of the Kolmogorov timescale. This behavior is essentially a kinematic effect due to fast rotations. Remember that $\dot{\gamma}$ is obtained by projecting the velocity shear on the direction $\mathbf{p}$ of a rigid rod. This direction rotates with an angular speed given by the vorticity $\omega = |\nabla \times \boldsymbol{u}|$, so that $\dot{\gamma}$ can alternate from expansion to compression, on timescales of the order of $\omega^{-1} \sim \tau_\eta$. Surprisingly, at longer times $t \gtrsim 4\tau_\eta$, the autocorrelation of $\dot{\gamma}^-$ changes regime and decreases much slower than an exponential. This contradicts the classical phenomenological vision that velocity gradients are purely a small-scale quantity with correlations spanning only the dissipative scales. For more than a decade in t within the
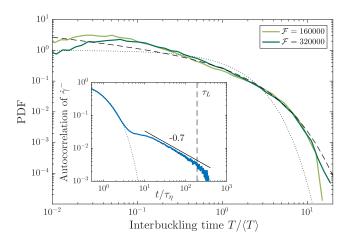

FIG. 3. Probability density functions [PDF (solid lines)] of the time T between successive buckling events, normalized to its average $\langle T \rangle \approx 52\tau_\eta$ for $\mathcal{F} = 1.6 \times 10^5$, and $\langle T \rangle \approx 36\tau_\eta$ for $\mathcal{F} = 3.2 \times 10^5$. The dotted line represents the exponential distribution. The dashed line is a Weibull distribution, Eq. (6), with shape $\beta = 0.7$ and scale parameter $\lambda = 1$. Inset: Autocorrelation $\rho(t) = \mathrm{cov}(\dot{\gamma}^-(t), \dot{\gamma}^-(0))/\mathrm{Var}(\dot{\gamma}^-)$ of the negative part of the stretching rate. The dotted line stands for $\exp(-t/\tau_\eta)$. The vertical dashed line indicates the large-eddy turnover time $t = \tau_L$. The solid line shows a slope -0.7.

inertial range, we indeed find a power-law behavior $\rho(t) \propto t^{-\beta}$, with $\beta \approx 0.7 \pm 0.1$. To our knowledge, this is the first time such a long-range behavior is observed for turbulent Lagrangian correlations.

These intricate correlations have important consequences on the incidence of buckling. Memory effects are present, as the fiber is likely to bend several times when in a clump of violent, high-frequency fluctuations of $\dot{\gamma}$. Consequently, the probability distribution $p(T)$ of the time T between successive buckling events is not exponential. This is clear from the main panel of Fig. 3, where this distribution is shown for $\mathcal{F} = 1.6 \times 10^5$ and 3.2×10^5. One observes deviations from the exponential distribution (dotted line). They relate to the two regimes discussed above for the time correlations of $\dot{\gamma}^-$. First, the distribution of interbuckling times is maximal for T of the order of τ_η. This corresponds to rapid oscillations of the sign of $\dot{\gamma}$. The fiber experiences several tumblings in an almost-constant velocity gradient and is alternatively compressed and pulled out by the flow due to fast rotations. This leads to a rapid succession of bucklings and straightenings. Second, strong deviations to the exponential distribution also occur for interbuckling times T in the inertial range. As seen in Fig. 3, the distribution of interbuckling times in the intermediate range $0.5 \lesssim T/\langle T \rangle \lesssim 5$ is well approximated by a Weibull distribution with shape β and scale parameter λ:

$$p(T) \approx \frac{\beta T^{\beta-1}}{\lambda^\beta} e^{-(T/\lambda)^\beta}. \qquad (6)$$

This decade exactly matches the time lags for which $\dot{\gamma}$ displays long-range correlations, that is, $\rho(t) \sim t^{-\beta}$. The return statistics of processes with power-law correlations is indeed expected to be well approximated by a Weibull distribution [24]. Longer times correspond to $t \gtrsim \tau_L$, for which $p(T)$ is expected to ultimately approach an exponential tail.

To characterize further buckling events and in particular their geometry, we show in Fig. 4 the joint probability density of the end-to-end length R and of the fiber's mean curvature, $\bar{\kappa} = (1/\ell) \int |\partial_s^2 X| ds$. The distribution is supported in a thin strip aligned with $\bar{\kappa} \propto (1 - R/\ell)^{1/2}$. Bucklings correspond to loops in this plane. Trajectories typically start such excursions with a larger curvature (upper part of the strip) than the one they have when relaxing back to a straight configuration (lower part). The orange curve corresponds to the first buckling event of the trajectory shown in Fig. 1. The curvature increases concomitantly to a decrease of the end-to-end length. Right before reaching a maximal bending, the fiber displays several coils (top left inset). This configuration depends on the most unstable mode excited with the current value of the instantaneous flexibility $\mathcal{F}_{\text{loc}}$. It is indeed known that buckling fibers in steady shear flows can experience several
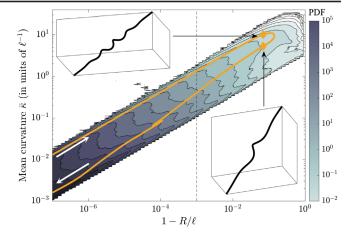

FIG. 4. Contour levels of the joint distribution of the end-to-end length R and of the mean curvature $\bar{\kappa}$ for $\mathcal{F} = 1.6 \times 10^5$. The vertical dashed line shows the threshold $R/\ell = 0.999$. An excursion of the same trajectory as Fig. 1 is shown for $43 < t/\tau_\eta < 77$ (orange). Also, two instantaneous configurations of the fiber are represented for $t = 43\tau_\eta$ (top left inset) and $t = 45\tau_\eta$ (bottom right inset).

bifurcations, depending on their elasticity [7]. Once the fiber has again aligned with $\dot{\gamma} > 0$, that is, a couple of τ_η's later, these coils unfold (bottom right inset), the curvature decreases, and the fiber relaxes back to a straight configuration. This specific event has been chosen for its simplicity and representativity. Still, it experiences a nontrivial episode at $1 - R \approx 10^{-4}$, during which the fiber configuration seems frozen. This event corresponds to the plateau observed in the top of Fig. 1 for $50\tau_\eta < t < \approx 80\tau_\eta$, right after the maximum of buckling. At these instants of time, $\dot{\gamma}$ is weakly oscillating around zero and the fiber is neither compressed nor stretched by the flow.

To conclude, recall that we have focused on passively transported fibers. In several applications, they actually have an important feedback on the flow and might even reduce turbulent drag. We found here that the dynamics of flexible fibers strongly depends on the shear strength: In calm regions, they just behave as stiff rods; in violent, intermittent regions, they can buckle, providing an effective transfer of kinetic energy toward bending elasticity. Such nonuniform, shear-dependent effects likely lead to intricate flow modifications, where the presence of small fibers affects not only the amplitude of turbulent fluctuations but also their very nature. Such complex non-Newtonian effects undoubtedly lead to novel mechanisms of turbulence modulation.

---

[1] P.-G. de Gennes, *Scaling Concepts in Polymer Physics* (Cornell University Press, Ithaca, NY, 1979).

[2] T. Watanabe and T. Gotoh, Phys. Rev. E **81,** 066301 (2010).

[3] A. S. Pereira, G. Mompean, L. Thais, E. J. Soares, and R. L. Thompson, Phys. Rev. Fluids **2,** 084605 (2017).

[4] F. Lundell, L. D. Söderberg, and P. H. Alfredsson, Annu. Rev. Fluid Mech. **43,** 195 (2011).

[5] M. N. Ardekani, G. Sardina, L. Brandt, L. Karp-Boss, R. Bearon, and E. Variano, J. Fluid Mech. **831,** 655 (2017).

[6] V. Smetacek, Protistologica **150,** 25 (1999).

[7] L. E. Becker and M. J. Shelley, Phys. Rev. Lett. **87,** 198301 (2001).

[8] A. Lindner and M. Shelley, *Fluid-Structure Interactions in Low-Reynolds-Number Flows* (Royal Society of Chemistry, London, 2015), pp. 168–192.

[9] A.-K. Tornberg and M. J. Shelley, J. Comput. Phys. **196,** 8 (2004).

[10] M. Harasim, B. Wunderlich, O. Peleg, M. Kröger, and A. R. Bausch, Phys. Rev. Lett. **110,** 108302 (2013).

[11] Y. Liu, B. Chakrabarti, D. Saintillan, A. Lindner, and O. du Roure, Proc. Natl. Acad. Sci. U.S.A. **115,** 9438 (2018).

[12] Y.-N. Young and M. J. Shelley, Phys. Rev. Lett. **99,** 058303 (2007).

[13] E. Wandersman, N. Quennouz, M. Fermigier, A. Lindner, and O. Du Roure, Soft Matter **6,** 5715 (2010).

[14] V. Kantsler and R. E. Goldstein, Phys. Rev. Lett. **108,** 038103 (2012).

[15] C. M. Schroeder, R. E. Teixeira, E. S. G. Shaqfeh, and S. Chu, Phys. Rev. Lett. **95,** 018301 (2005).

[16] E. Plan and D. Vincenzi, Proc. R. Soc. A **472,** 20160226 (2016).

[17] H. Homann, J. Dreher, and R. Grauer, Comput. Phys. Commun. **177,** 560 (2007).

[18] R. Ni, N. T. Ouellette, and G. A. Voth, J. Fluid Mech. **743** R3 (2014).

[19] C. Brouzet, G. Verhille, and P. Le Gal, Phys. Rev. Lett. **112,** 074501 (2014).

[20] M. Rosti, A. Banaei, L. Brandt, and A. Mazzino, Phys. Rev. Lett. **121,** 044501 (2018).

[21] G. Boffetta, A. Celani, and S. Musacchio, Phys. Rev. Lett. **91,** 034501 (2003).

[22] P. Kailasnath, K. R. Sreenivasan, and G. Stolovitzky, Phys. Rev. Lett. **68,** 2766 (1992).

[23] D. Buaria, A. Pumir, E. Bodenschatz, and P. Yeung, in *APS Meeting Abstracts* (American Physical Society, New York, 2017).

[24] J. F. Eichner, J. W. Kantelhardt, A. Bunde, and S. Havlin, Phys. Rev. E **75,** 011128 (2007).